PAUL SCHERRER INSTITUT

SLS-TME-TA-1998-0003
26. Februar 1998

SLS dynamic aperture with minigap insertion devices

L. Tosi

Sincrotrone Trieste

A. Streun

PSI

Introduction

The initial experimental equipment of the Swiss Light Source will comprise beamlines for protein crystallography (area X06S), materials science (X04S), surfaces and interfaces (X09L), micro- and nanostructures (X10D) and a generic beamline (X07M) [1].

The generic beamline will use a common undulator U38 (38 mm period) and the micro and nanostructures beamline will use a bending magnet.

Materials science experiments require a large flux of photons up to 40 keV to be produced from the wiggler W40. The protein crystallography requires high brightness up to 17.5 keV, to be produced by the undulator U19 (21^{st} harmonic at 2.1 GeV or 15^{th} at 2.4 GeV). Both U19 and W40 will have very small gaps of approx. 4 mm full height.

The surfaces and interfaces beamline requires fast switchable circular polarisation for experiments on circular dichroism, to be produced by the electromagnetic long elliptical wiggler EW200.

Due to their heigh field (U19, W40) and significant multipole content (U19, W40, EW200) these advanced insertion devices affect the stability of the stored electron beam by breaking the lattice symmetry (linear effect) and by exciting higher order betatron resonances (nonlinear effect).

The program RACETRACK [2] was used to investigate the dynamic aperture of SLS in the presence of these advanced insertion devices.

Dynamic apertures of the ideal lattice

The dynamic aperture of the SLS storage ring [3] had been optimized by minimizing the sextupole Hamiltonian up to second order in sextupole strength [4] as implemented in the program OPA [5].

Figures A1 and A2 show the horizontal and vertical dynamic and physical aperture as a function of relative momentum deviation dp/p for the ideal lattice (i.e. no magnet errors, no insertion devices, no synchrotron oscillations) in the operation mode with dispersion free straight sections. The beampipe as used for physical aperture calculation was assumed to have everywhere a full width of 65 mm and a full height of 35 mm.

Figure A3 shows the momentum dependant beta functions and tunes. Apertures and beta functions are shown at the centre of the long straight sections, which was the trackpoint for all calculations.

Figure A4 shows the working point in the tune diagram with resonances up to sixth order for the ideal lattice with a periodicity of 3, and for the lattice with broken periodicity. The proximity of a first order sextupole (= third order betatron) resonance indicates already here, that this lattice configuration might be vulnerable by symmetry breaking from the installation of a strong insertion device. Hence, it is important to evaluate what the consequences might be by computing the dynamic aperture with insertion devices.

Description of the insertion devices

U19 is a permanent magnet undulator of 102 periods and length 1.938 m, reaching a peak field on axis of B_o = 1.2 T at a full gap height of 4 mm.

W40 is a superconducting wiggler of 50 periods and length 2.0 m, reaching a peak field on axis of B_o = 2.1 T at a full gap height of 4 mm.

EW200 is an electromagnetic elliptic wiggler with each 45 horizontal and vertical periods. The on axis peak fields are B_o = 0.35 T in the vertical and B_o' = 0.22 T in the horizontal at a full gap height of 20 mm.

Tracking parameters

In order to investigate effects on the dynamic aperture due to the introduction of the devices into the storage ring, four particles with different initial conditions were tracked over 500 or 1000 turns with the code RACETRACK [2]. As a preliminary computation, a comparison of the dynamic apertures in the lattice without insertion devices computed by the two programs RACETRACK and OPA was performed showing a very good overall agreement (Fig. U1 to U3). The plots show only one quadrant, with the (–x,y) quadrant reflected to positive x-values and the lower value taken as aperture data. In the vertical the machine is mirror symmetric anyway (see fig. A2).

For each investigated insertion device tracking was performed for an energy of 2.1 GeV and for energy deviations of ±4% and of ±5%. The observation point of the tracked particles was taken to be at the centre of a long straight. The mini-gap insertion devices are planned to be situated centered in the short (U19, W40) and in the long straight (EW200). The beta function at the trackpoint and at the *edge* of the insertion, given by $\beta = \beta_o + (L/2)^2/\beta_o$ with β_o the beta function in the centre of the corresponding straight section and L the Length of the insertion, were used to transform the physical aperture restriction from the beampipe and from the insertion's gap to the trackpoint.

The following table displays the beta functions at long and short straight centres (where $\alpha_x = \alpha_y = \eta' = 0$ and $\eta = 0$) for the five values of momentum used in the calculations (also see figure A3 for the long straight beta functions):

dp/p	**0 %**	**– 4 %**	**– 5 %**	**+ 4 %**	**+ 5 %**
Long straight β_x [m]	4.14	5.79	6.26	2.81	2.67
Long straight β_y [m]	6.10	4.63	4.34	7.39	7.53
Short straight β_x [m]	1.18	1.50	1.63	1.15	1.13
Short straight β_y [m]	2.61	1.77	1.66	4.24	4.81

Modelling of insertion devices

The magnetic field model used for the insertion device is [6]:

$B_x = B_o \, k_x/k_y \, sh\,(k_x x)\, sh\,(k_y y)\, cos\,(kz) + B_o' \, ch\,(k_x' x)\, ch\,(k_y' y)\, sin\,(kz)$

$B_y = B_o \, ch\,(k_x x)\, ch(k_y y)\, cos\,(kz) + B_o' \, k_y'/k_x' \, sh\,(k_x' x)\, sh\,(k_y' y)\, sin\,(kz)$

$B_z = -B_o \, k/k_y \, ch\,(k_x x)\, sh\,(k_y y)\, sin\,(kz) + B_o' \, k/k_x' \, sh\,(k_x' x)\, ch\,(k_y' y)\, cos\,(kz)$

where $k_x^2 + k_y^2 = k_x'^2 + k_y'^2 = k^2 = (2\pi/\lambda_o)^2$ with λ_o the period length of the device.

The motion of the particles throughout the device is derived using a second order symplectic integration scheme [7].

Not having at the moment any available data on the actual transverse variation of the fields, computations were done twice for the mini-undulator and for the wiggler. In one case infinite

pole widths, in which the devices act as a drift in the horizontal plane, were assumed and in the other case the devices defocused weakly in the horizontal plane. These two cases correspond to taking $k_x = 0.0$ and $k_x^2 = -0.01\ k^2$. Results showed that there were not significant differences between the dynamic apertures in the two cases. Due to the maximum on axis field values and to the period lengths of the two mini-gap devices, dynamic aperture computations were done also treating the devices as linear elements in order to distinguish the effects due to linear optical distortions from those due to the non-linearities of the devices.

For the elliptical device located in a long straight, computations were first done using the transverse propagation constants $k_x^2 = -42.3\ m^{-1}$ and $k'^2_x = 1003.6\ m^{-1}$.

In order to give an idea of what the impact might be of a transverse field distribution which does not follow a hyperbolic law, tracking was also done for a polynomial field variation [8] using the coefficients obtained for the electromagnetic elliptical wiggler installed at ELETTRA.

Results for undulator U19

Figures U1 to U5 show the dynamic apertures for on and off momenta particles when U19 is introduced in the lattice. The results show a strong impact of the device on the dynamic aperture of the machine especially at large vertical amplitudes which was found to be due to the non-linearities of the device. However, it can be seen that the maximum stable amplitudes are still well above the physical aperture of the chamber. The linear distortions generated by the device gave a vertical tune shift of $\Delta\nu_y = 0.006$ and a maximum vertical beta beat of 5% in the straight sections.

Results for wiggler W40

Figures W1 to W5 show the results of the computations when the wiggler W40 is introduced in the lattice. In this case, a strong horizontal reduction is also observed. This was found to be caused by the symmetry break of the linear optics, as it can be observed from the results when treating the device as a linear element. The linear tune shift produced by the wiggler is $\Delta\nu_y = 0.018$ with a maximum vertical beta beat of 16% in the straights. Since the linear effects of insertion devices scale inversely with energy, a computation of the dynamic aperture was done for a machine energy of 2.4 GeV. As it can be seen in figure W6, the optical symmetry break is still strong enough to deteriorate the sextupole optimization. The linear tune shift in this case was $\Delta\nu_y = 0.014$.

Figure W7 show the dynamic aperture when both the wiggler W40 and the undulator U19 are present in the lattice.

Results for elliptical wiggler EW200

Figures E1 to E5 show the results of the simulations with the elliptical wiggler using the standard model with hyperbolic functions. The result looks very encouraging, the only significant impact being a sharp cut-off of the maximum horizontal amplitude, which is produced by non-linear coupling effects. The situation however is different when the device is modelled transversely by a polynomial and using the data found for the Elettra elliptical wiggler. The result is shown in figure E6.

Conclusion

The minigap insertion devices investigated do not seriously affect the dynamic aperture. Thus so far there is no objection against installation into the SLS storage ring. However the combined effect from insertion devices and magnet multipole errors, alignment errors, synchrotron oscillations etc. was not yet treated. Also the impact of small gaps on lifetime needs further investigation. The working point of the SLS lattice was found to be rather sensitive to breaking of lattice symmetry and has to be moved.

References:

[1] SLS Beamlines homepage:
http://www1.psi.ch/www_sls_hn/english/beamlines/sls_beamlines.htmlx

[2] F. Iazzourene et al., RACETRACK USER'S GUIDE, Sincrotrone Trieste Internal Report, ST/M-92/7

[3] The SLS Design Handbook, PSI 1998,
http://www1.psi.ch/www_slss_hr/docs/hbook/contents.htmlx

[4] J. Bengtsson, "The Sextupole Scheme for the Swiss Light Source (SLS): An Analytic Approach", SLS-TME-TA-1997-0009

[5] A. Streun, "OPA", http://www1.psi.ch/~betalib/opa.html

[6] R.P Walker, "Main Features of Electron Motion in General Helical Fields", Sincrotrone Technical Note, ST/M-TN-98/41.

[7] R. Nagaoka, L. Tosi, "An Improved Scheme for Integrating the Particle Motion through the Insertion Device in RACETRACK", Sincrotrone Internal Report, ST/M-90/6.

[8] L. Tosi et al., "Simulations of Non-linear Beam Dynamics Effects due to an Electromagnetic Elliptical Wiggler", PAC Conf. Proc, Vancouver, Canada, 1997

Figures

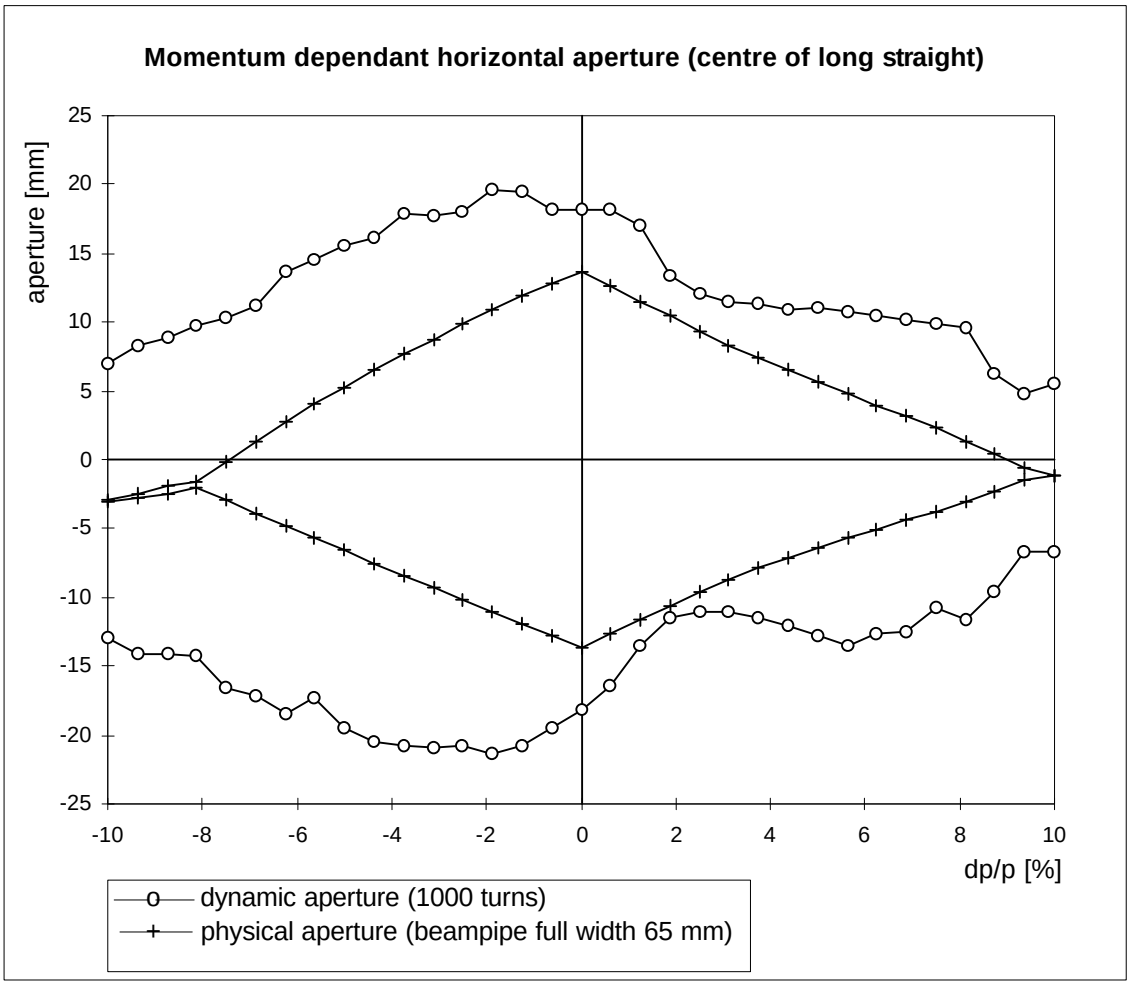

Figure A1: Horizontal dynamic and physical aperture at long straight centre as a function of relative momentum deviation for the ideal lattice (no synchrotron oscillations, no errors)

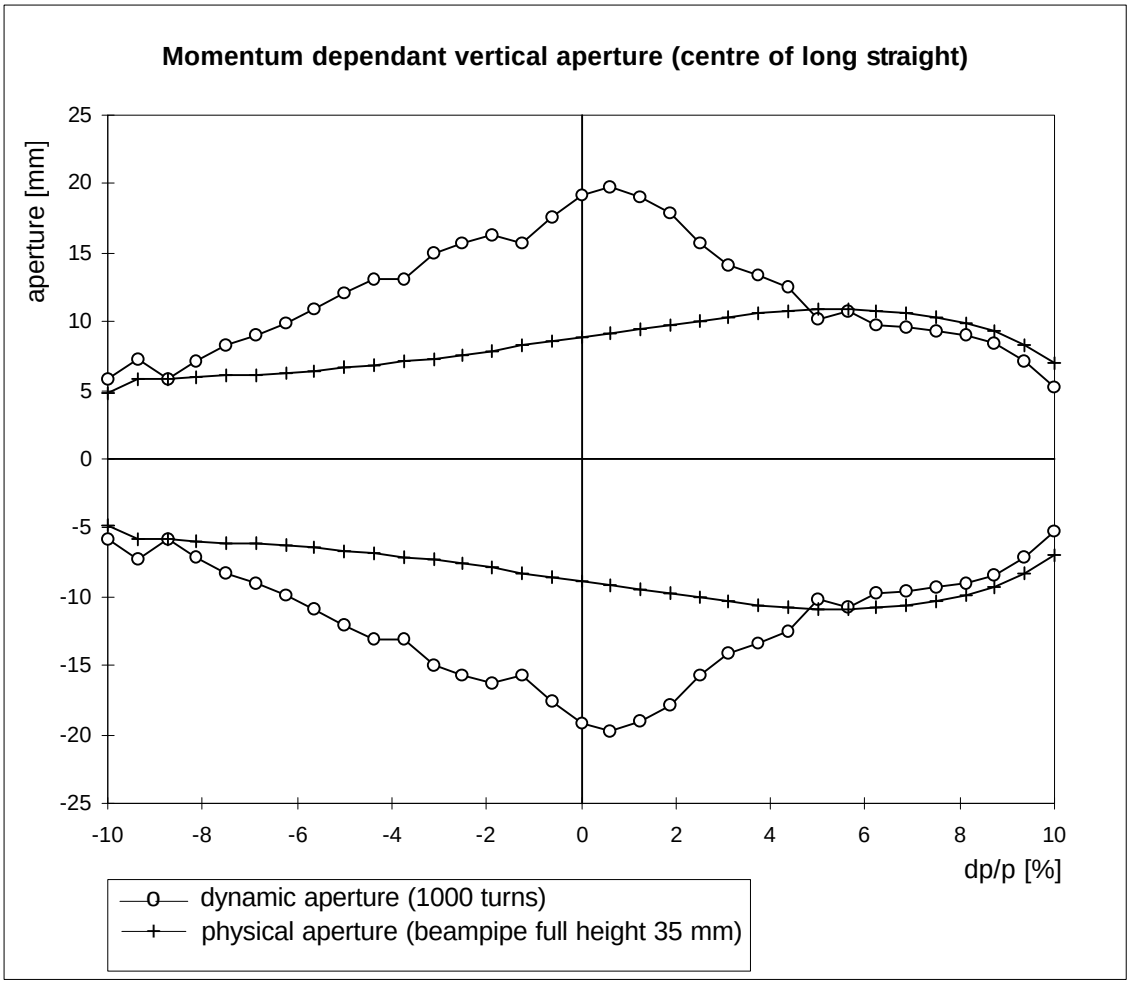

Figure A2: Vertical dynamic and physical aperture at long straight centre as a function of relative momentum deviation for the ideal lattice (no synchrotron oscillations, no errors).

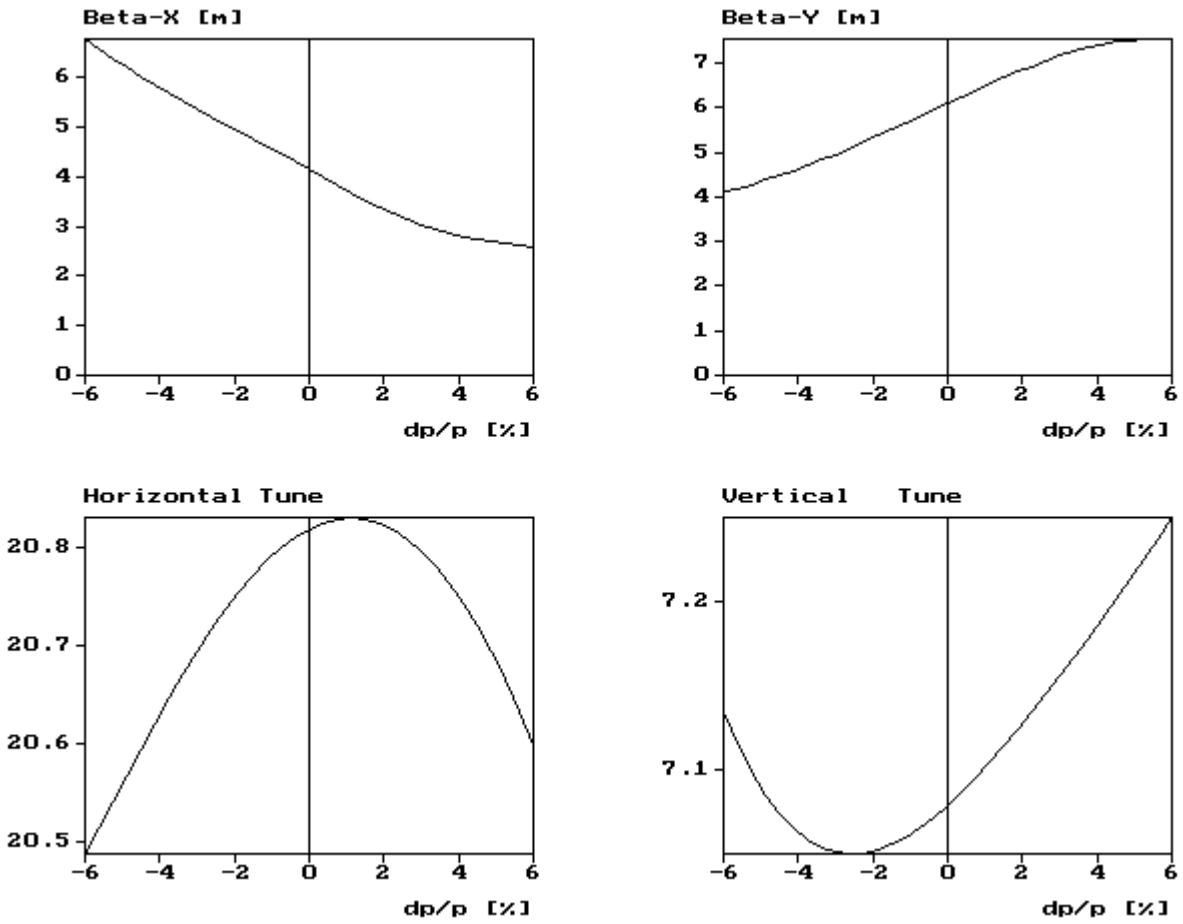

Figure A3: Momentum dependant beta functions (at centre of long straight) and tunes

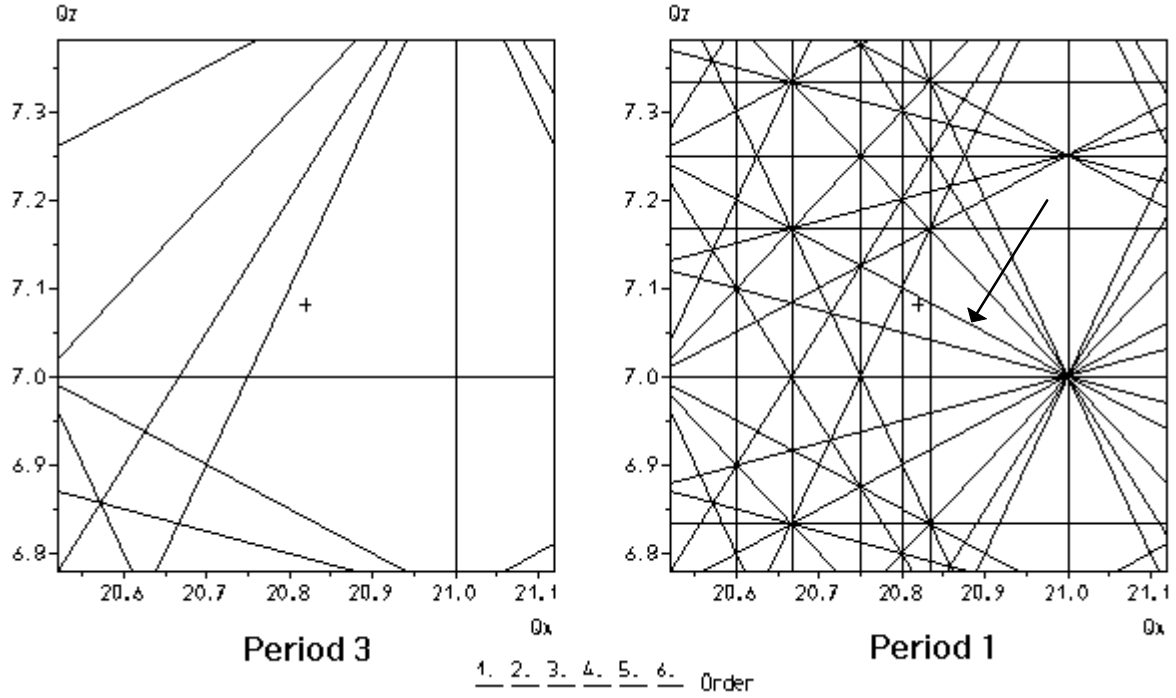

Figure A4: Tune diagram of the SLS lattice for period 3 and for period 1. The working point (+) at $\nu_x = 20.82$ and $\nu_y = 7.08$ chosen for the ideal lattice (period 3) is close to the first order sextupole resonance $\nu_x + 2\nu_y = 35$ becoming systematic after symmetry breaking (period 1).

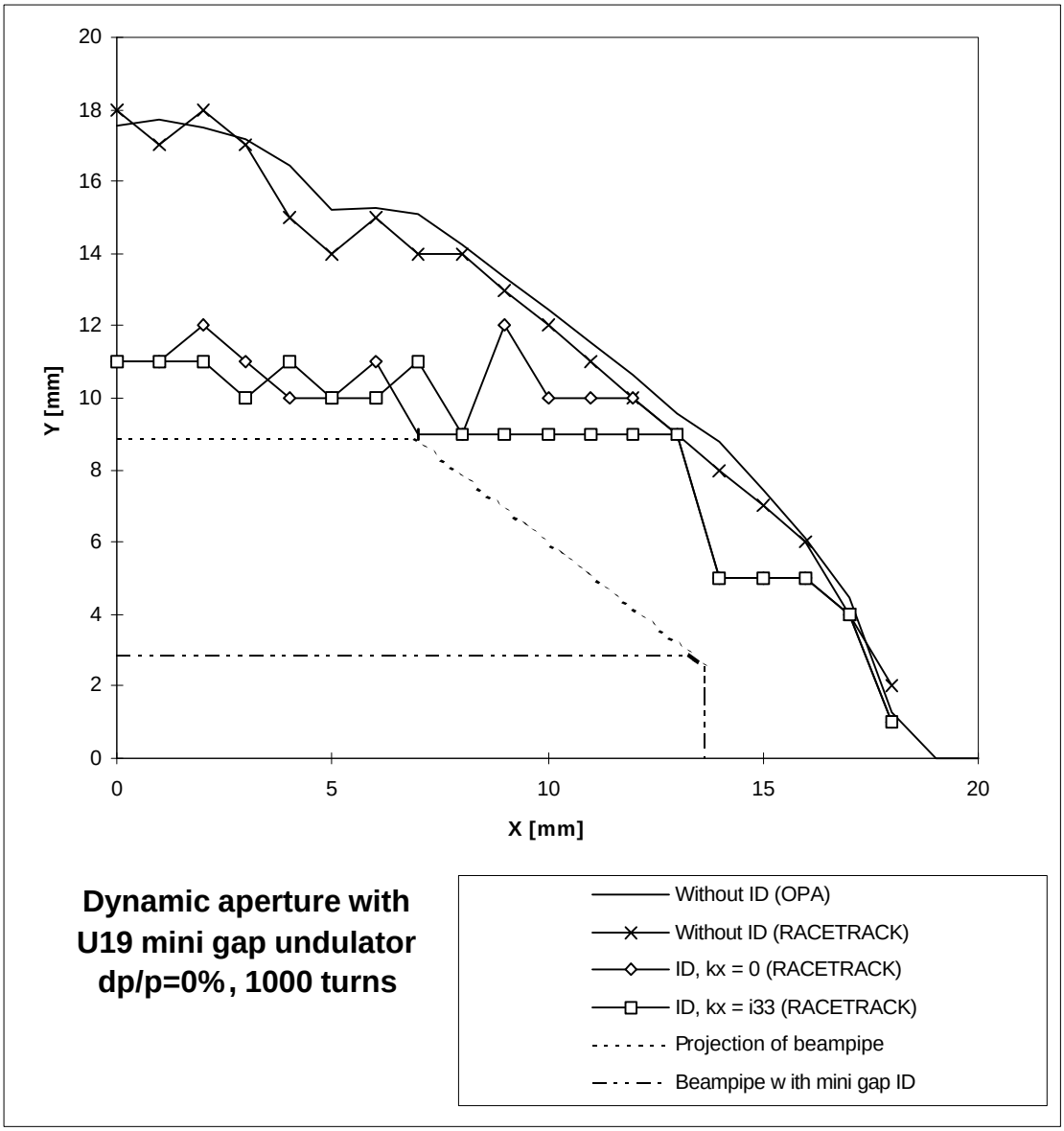

Figure U1: U19 mini gap undulator

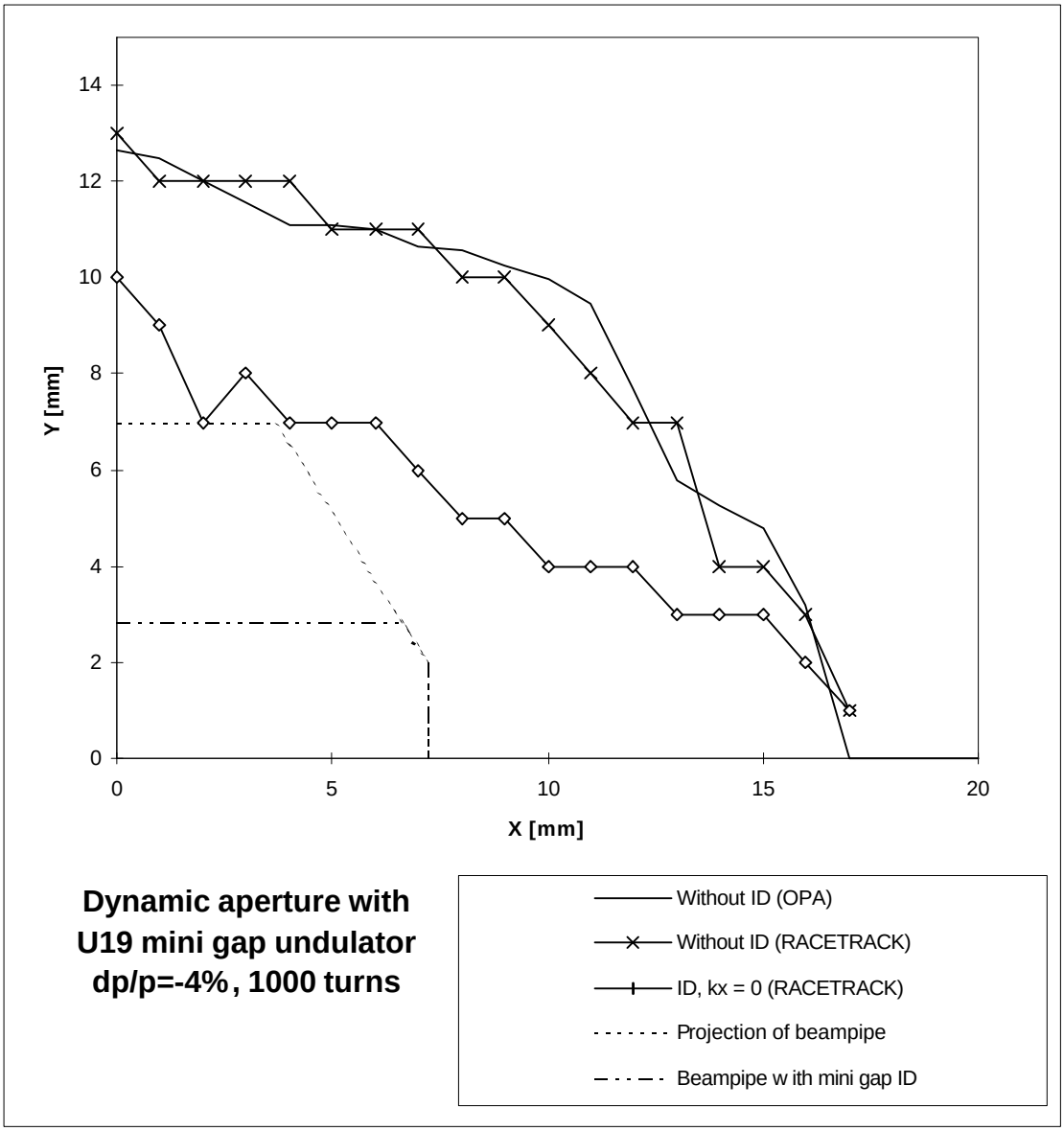

Figure U2: U19 mini gap undulator, dp/p = – 4 %

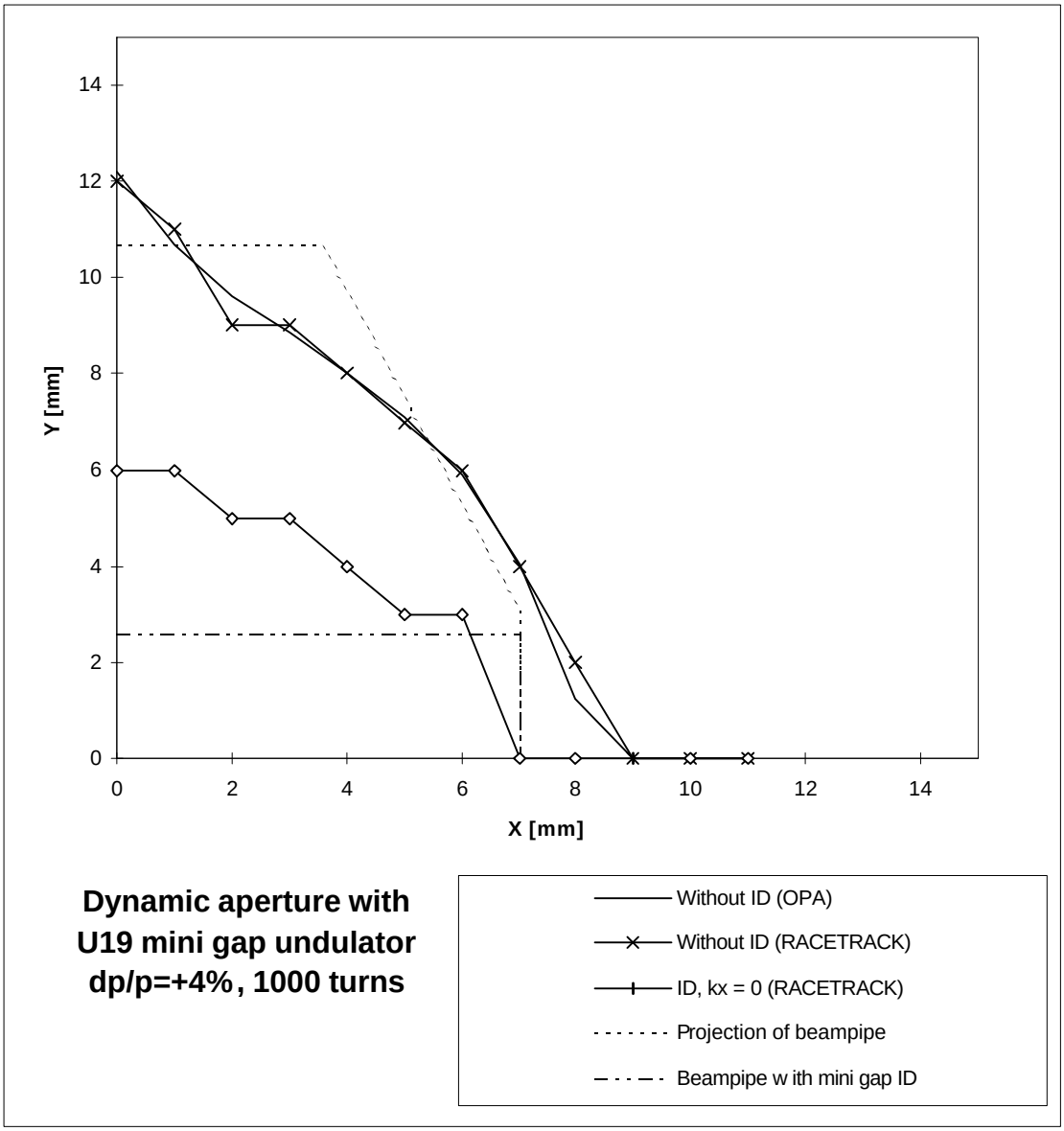

Figure U3: U19 mini gap undulator, dp/p = + 4 %

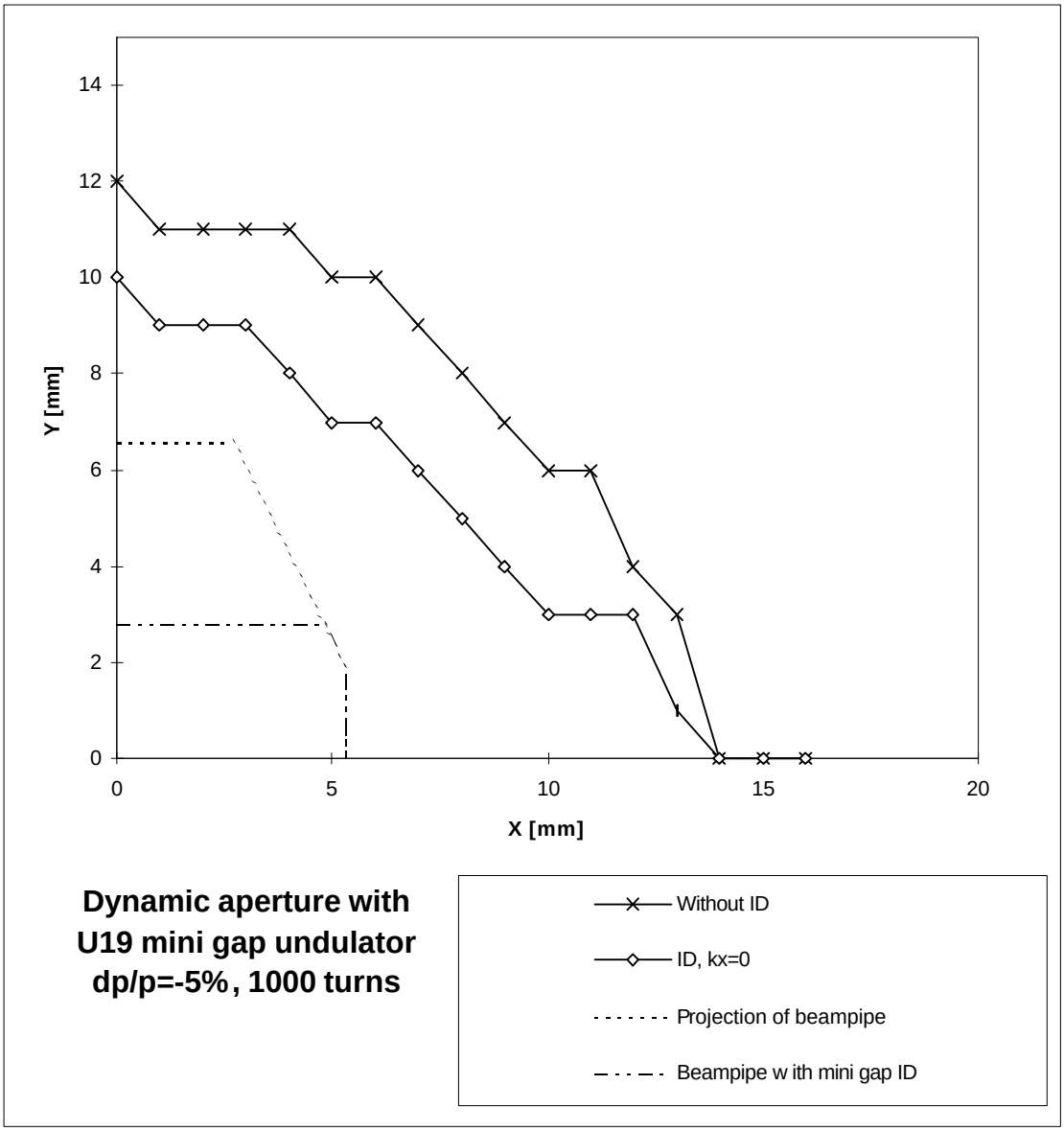

Figure U4: U19 mini gap undulator, dp/p = – 5 %

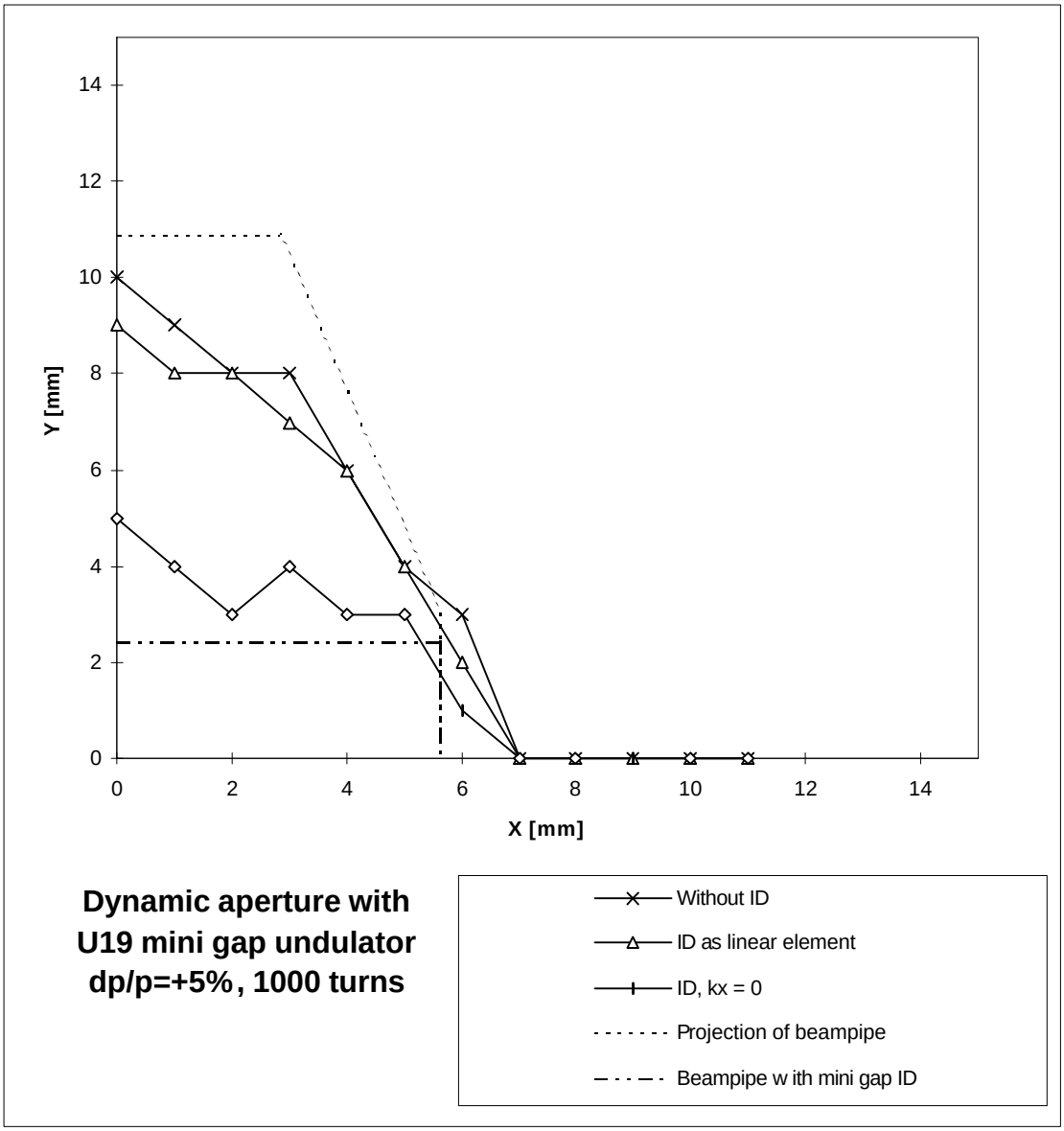

Figure U5: U19 mini gap undulator, dp/p = + 5 %

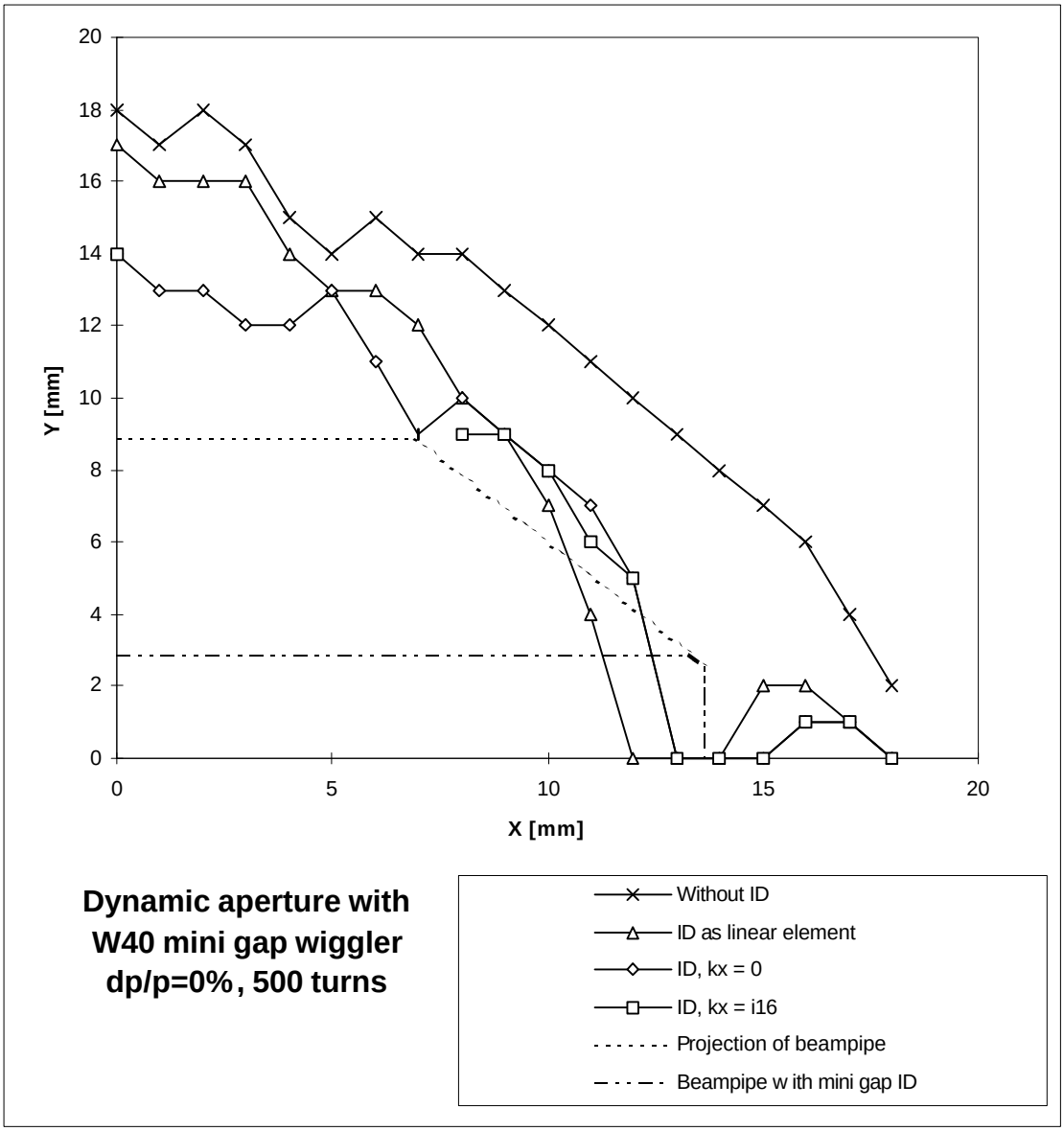

Figure W1: W40 mini gap wiggler

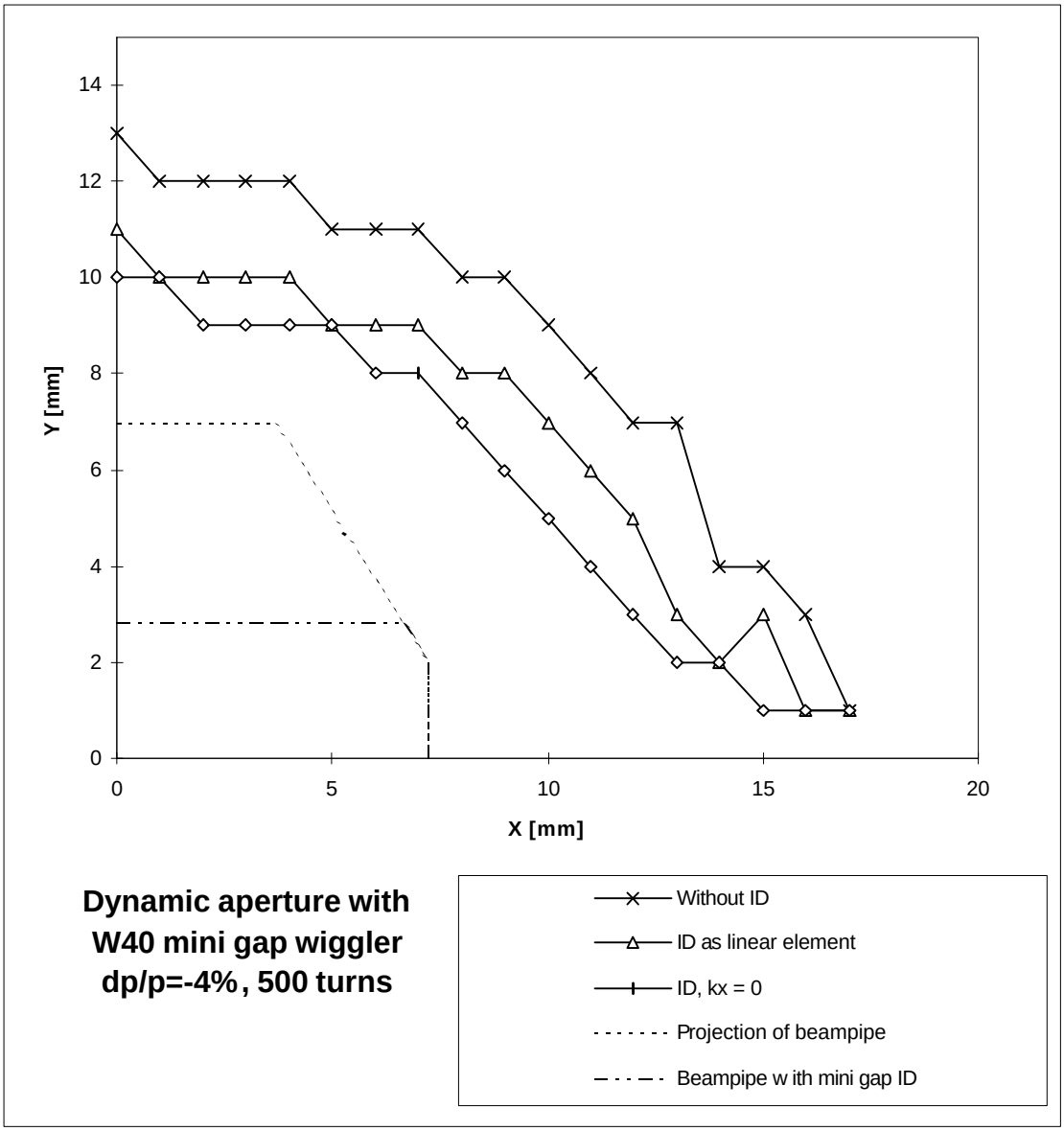

Figure W2: W40 mini gap wiggler, dp/p = – 4 %

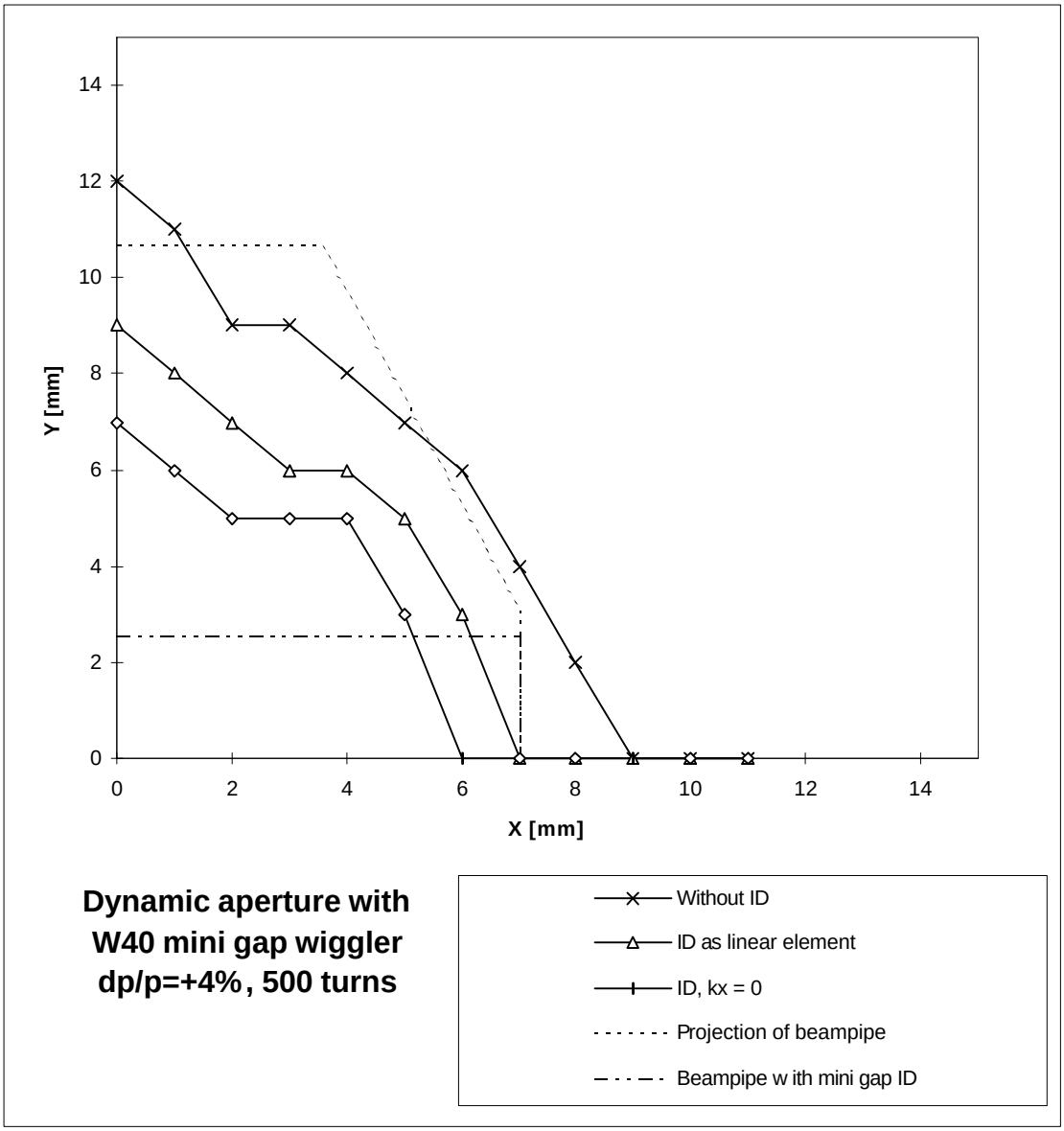

Figure W3: W40 mini gap wiggler, dp/p = + 4 %

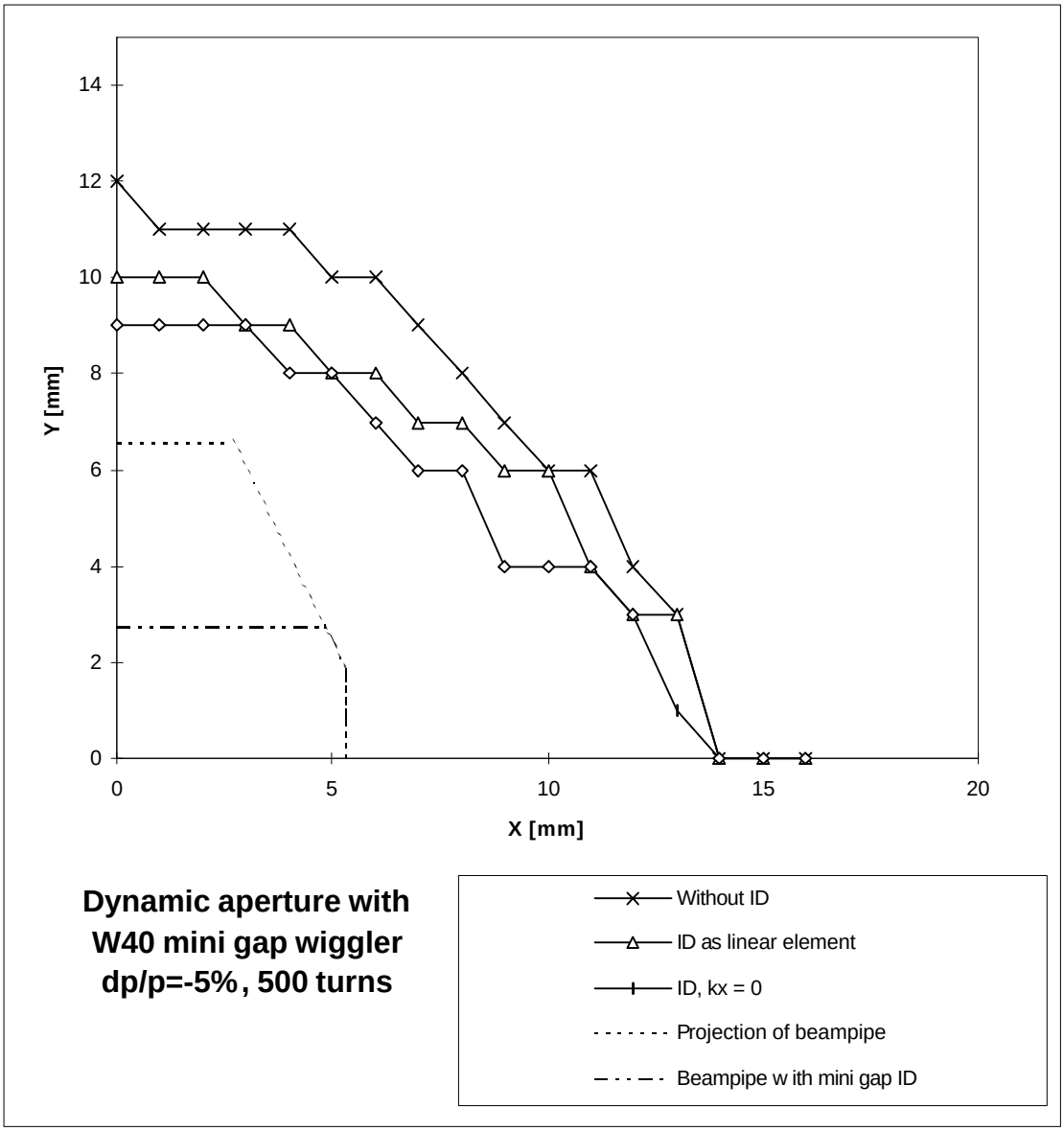

Figure W4: W40 mini gap wiggler, dp/p = – 5 %

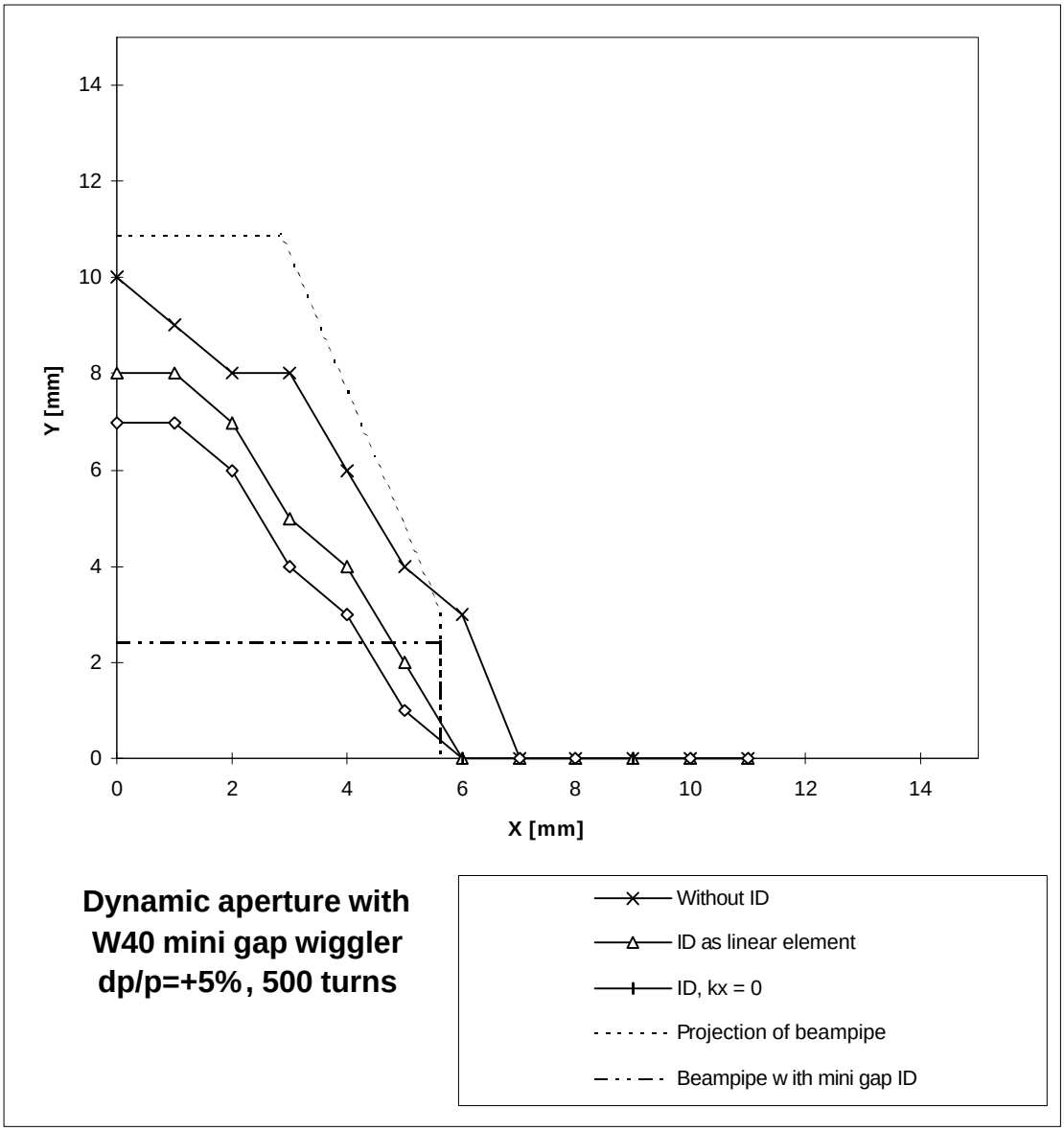

Figure W5: W40 mini gap wiggler, dp/p = + 5 %

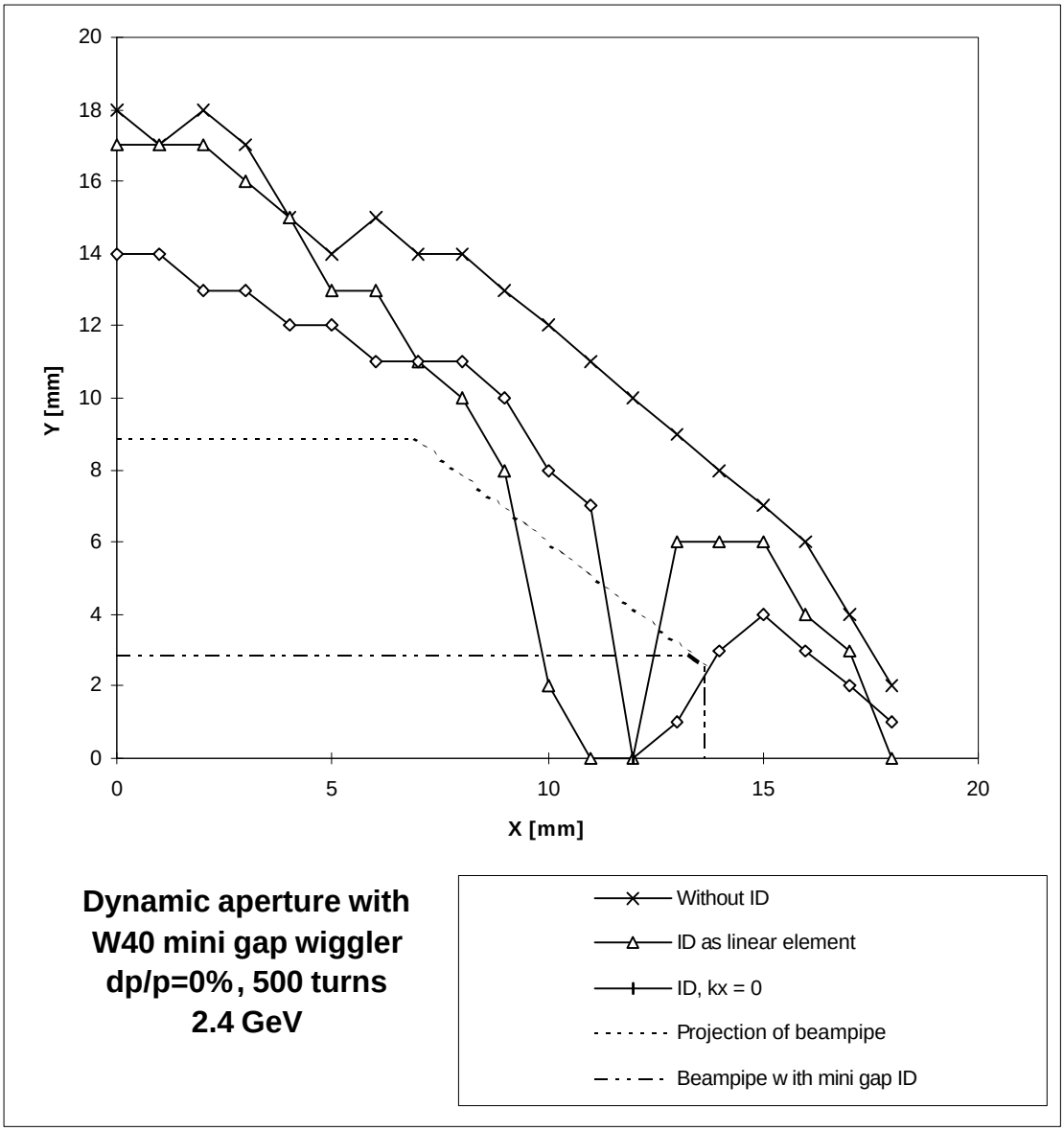

Figure W6: W40 mini gap wiggler at a beam energy of 2.4 GeV instead of 2.1 GeV

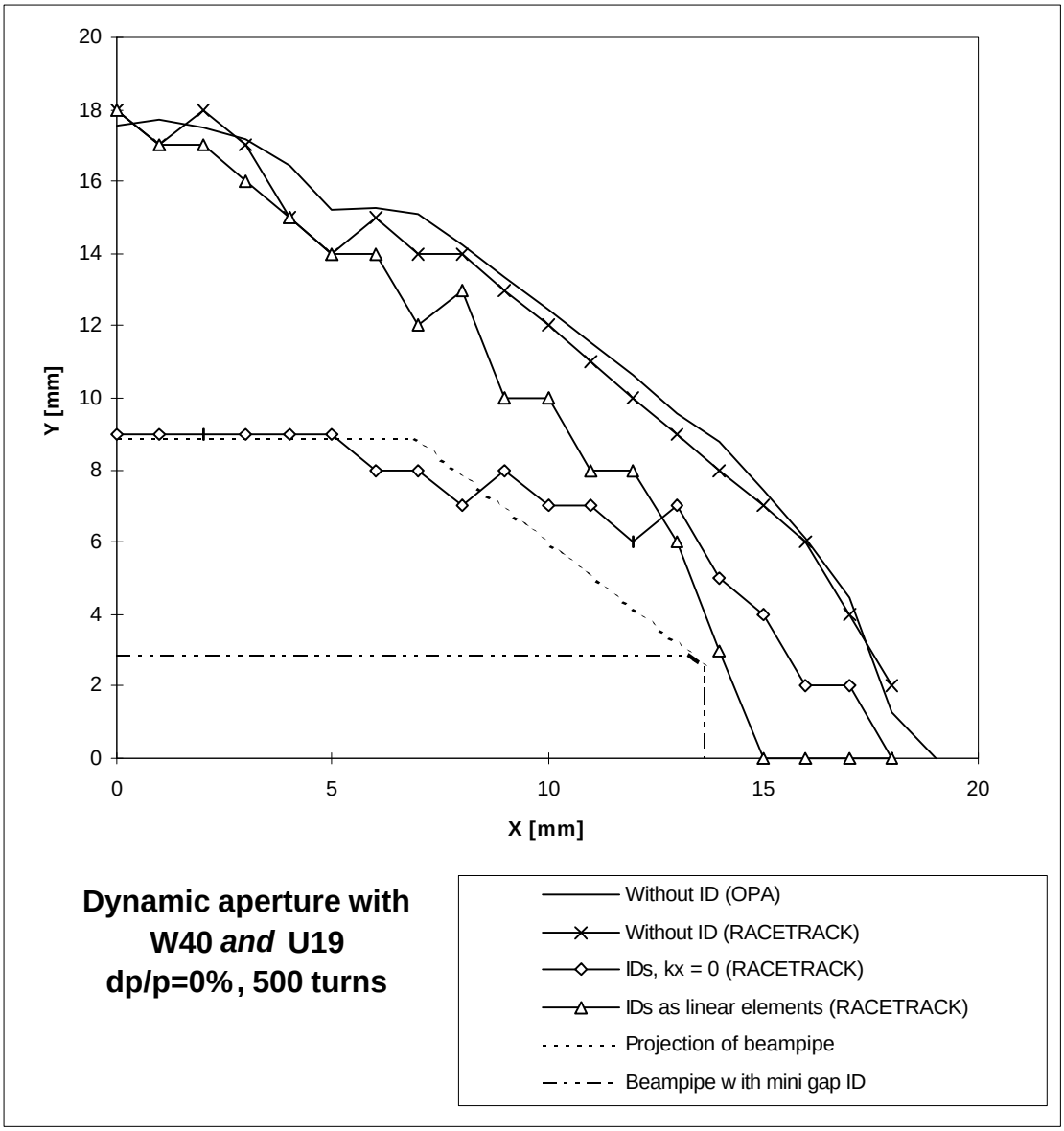

Figure W7: Combined effect of W40 mini gap wiggler and U19 mini gap undulator

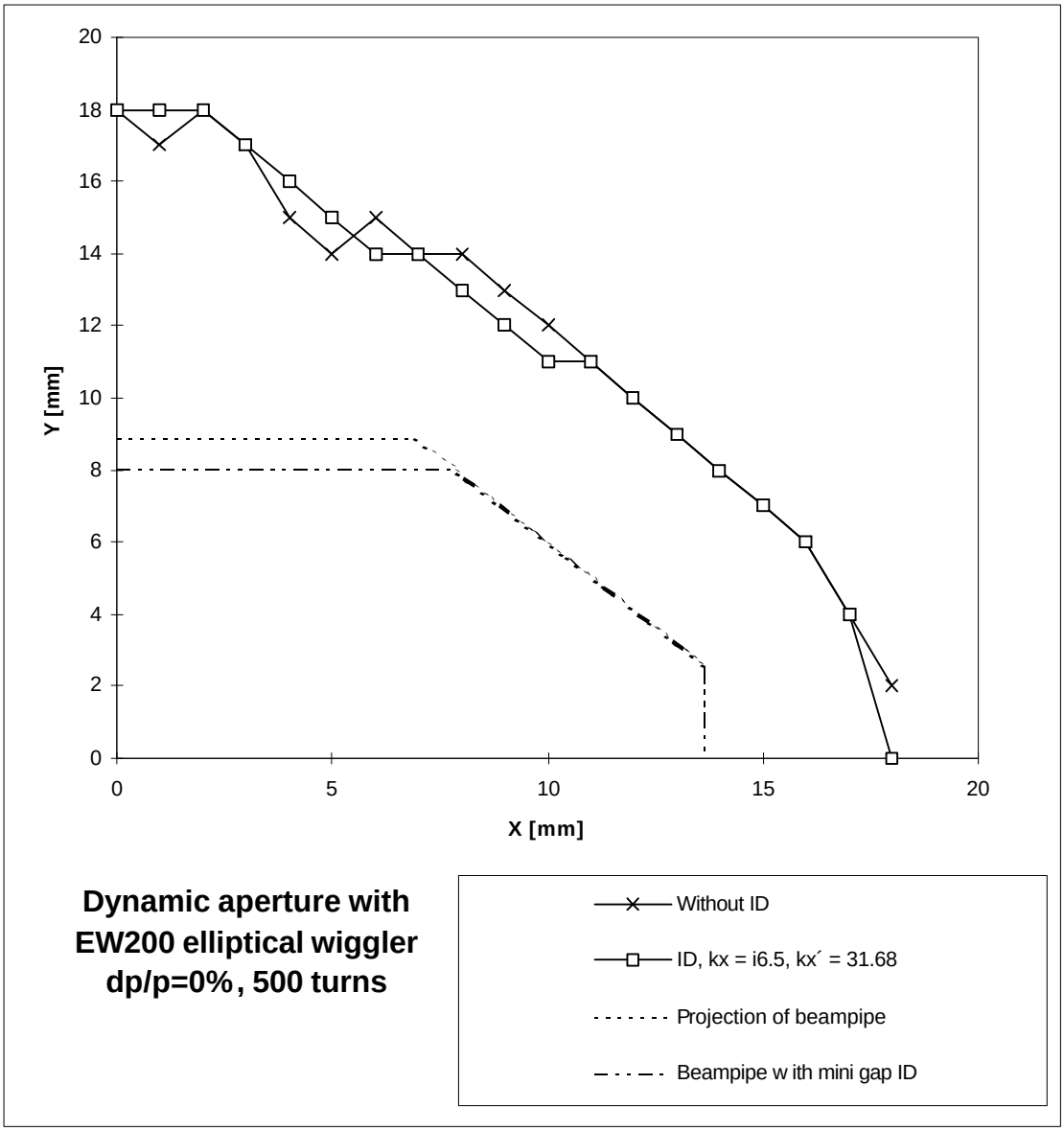

Figure E1: EW200 elliptical wiggler

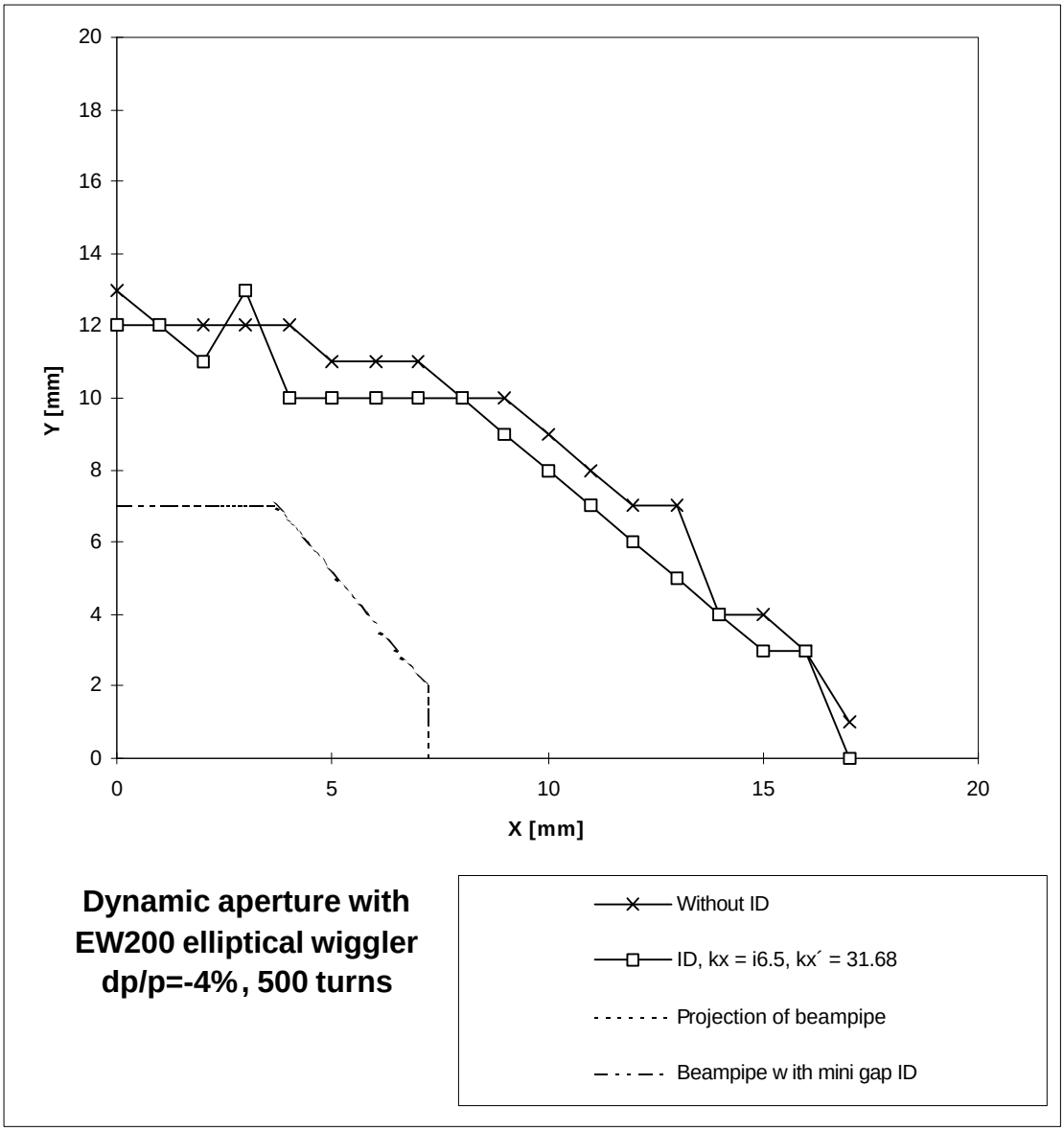

Figure E2: EW200 elliptical wiggler, dp/p = – 4 %

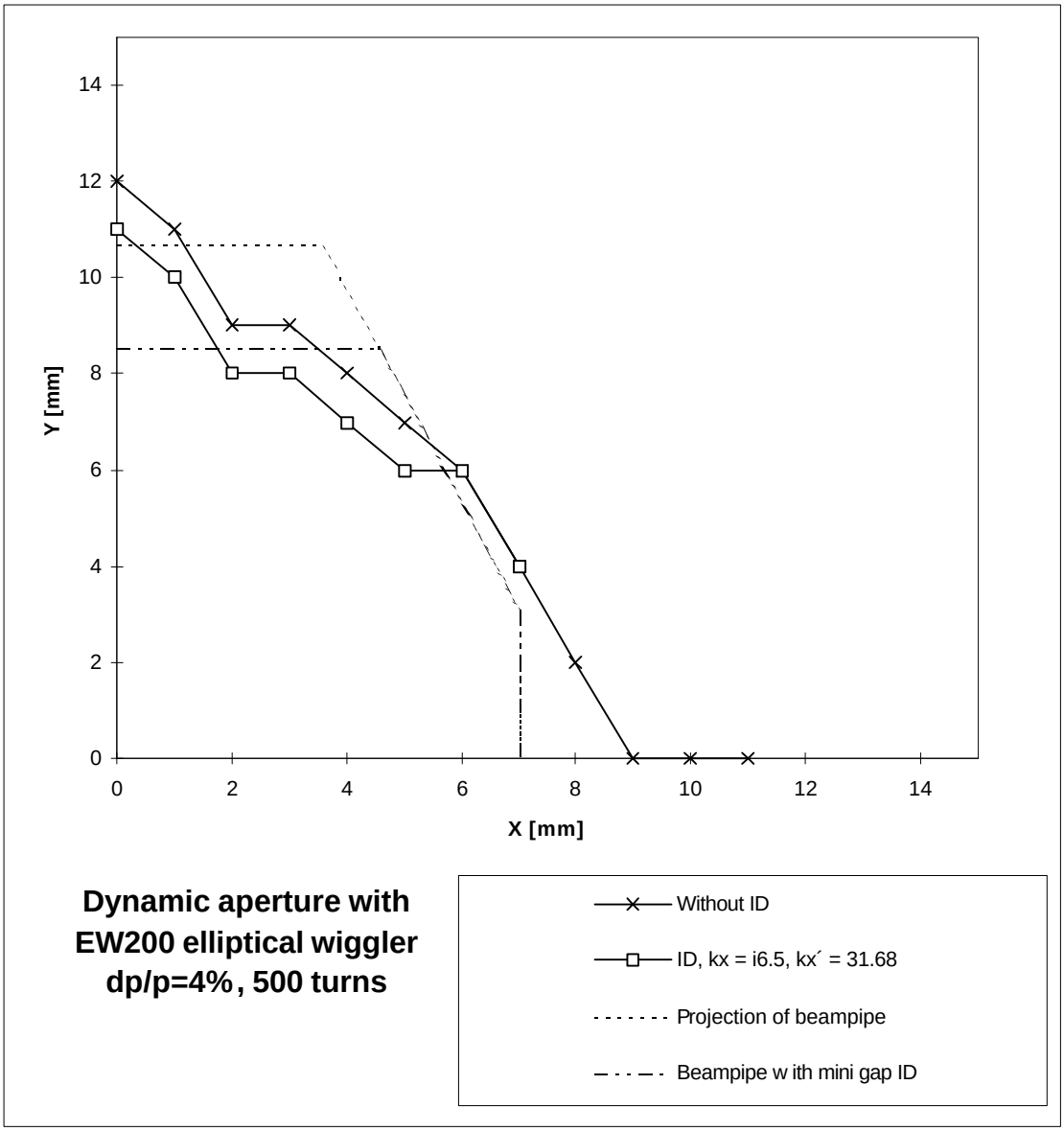

Figure E3: EW200 elliptical wiggler, dp/p = + 4 %

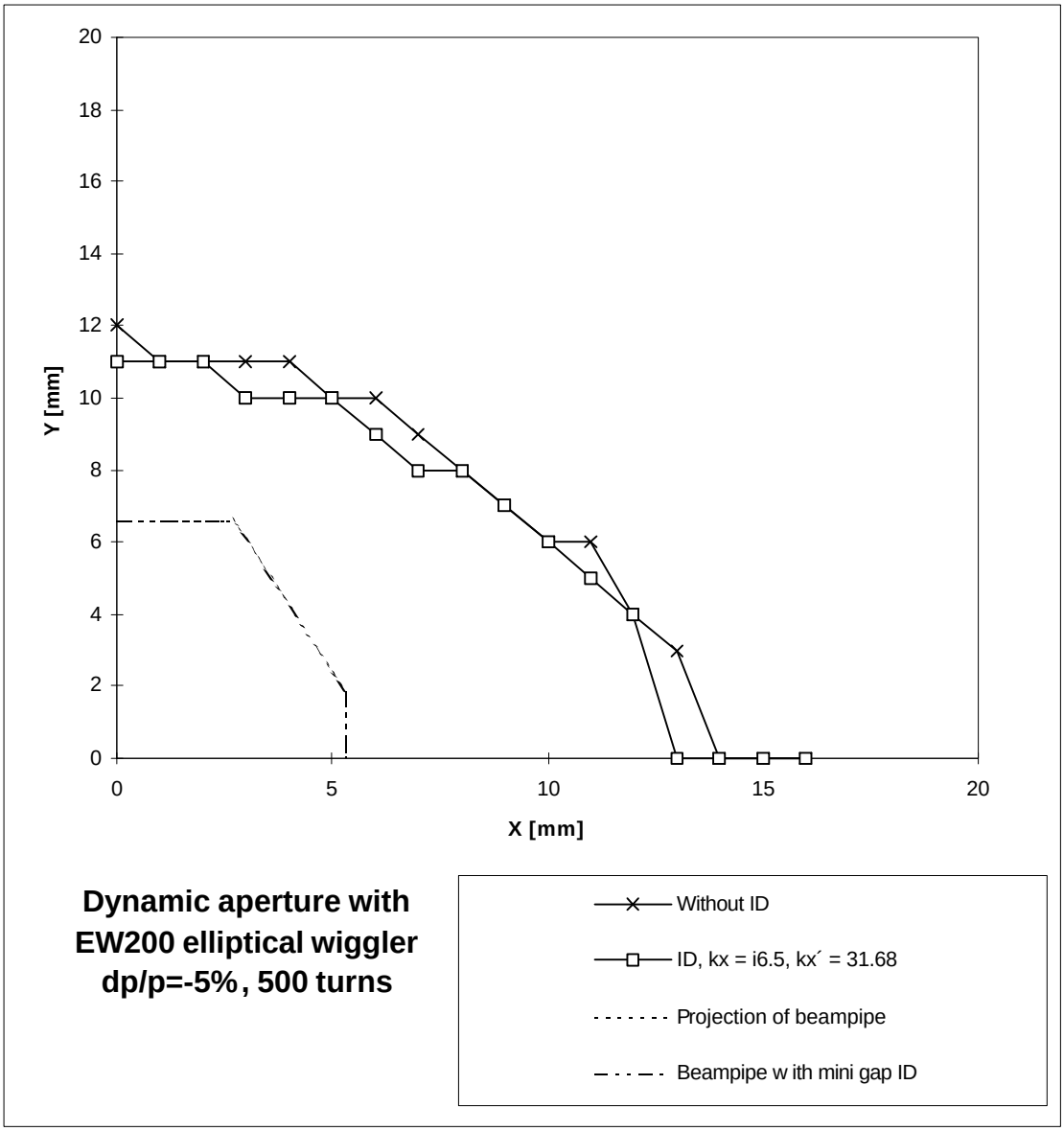

Figure E4: EW200 elliptical wiggler, dp/p = – 5 %

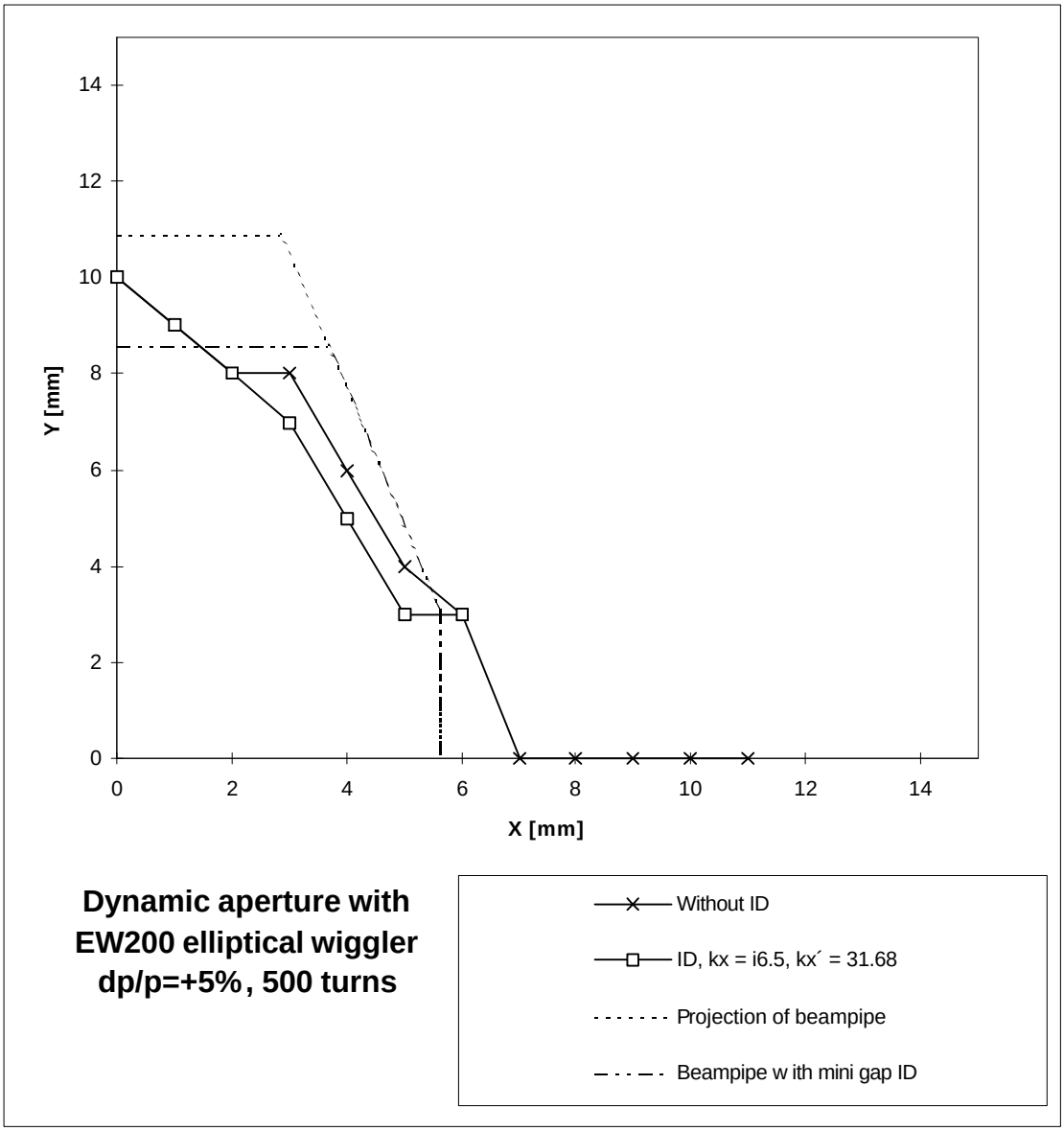

Figure E5: EW200 elliptical wiggler, dp/p = + 5 %

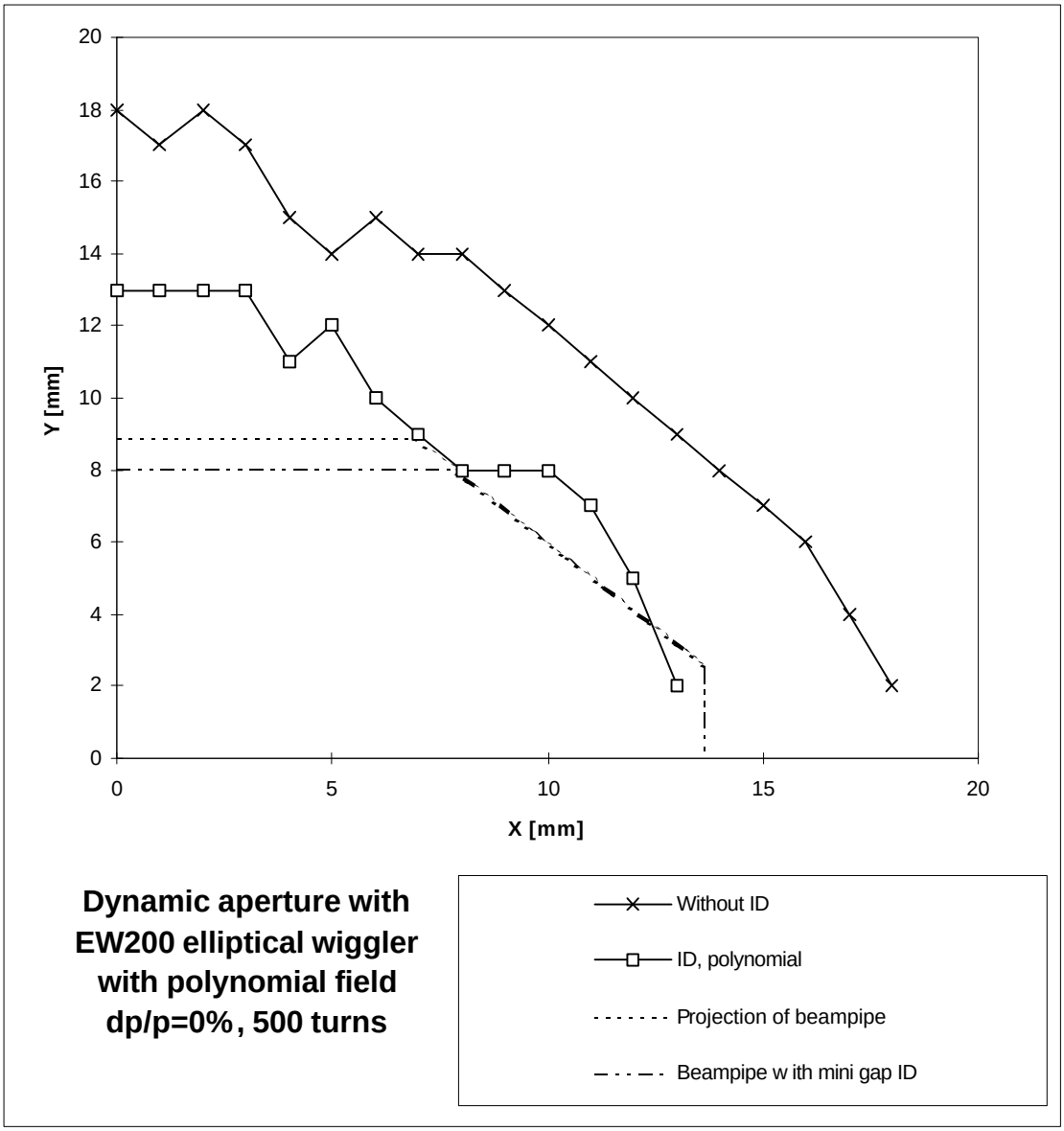

Figure E6: EW200 elliptical wiggler with polynomial field expansion as measured at ELETTRA